arXiv:astro-ph/9506048v1 7 Jun 1995

Rees-Sciama Effect in a CDM Universe

Uroš Seljak[1]
Department of Physics, MIT, Cambridge, MA 02139 USA

ABSTRACT

The Rees-Sciama (RS) effect produces fluctuations in the cosmic microwave background (CMB) through the time-dependent gravitational potential in the nonlinear stages of evolution. I investigate the RS effect on the CMB angular power spectrum C_l for several CDM models by combining the results of N-body simulations with second order perturbation theory. The amplitude of the RS fluctuations peaks at $l \sim 100 - 300$, where it gives $\Delta T/T \sim 10^{-7} - 10^{-6}$ for a wide range of models. This is at least an order of magnitude below the COBE normalized primary contribution. RS fluctuations could be a dominant source of anisotropies only on subarcminute scales ($l \approx 5000$) and are below the present day observational sensitivities on all angular scales.

Subject headings: cosmic microwave background—cosmology: large scale structure

1. Introduction

It is widely believed that cosmic microwave background anisotopies observed by COBE (Smoot et al. 1992) and smaller scale experiments are caused by small inhomogeneities in the matter distribution during the recombination epoch (redshift $z \approx 1100$). At that time the fluctuations were linear and in principle calculable with arbitrary precision, which would allow one to determine several cosmological parameters with a very high precision (e.g. Bond 1995; Hu & Sugiyama 1995; Seljak 1994). This picture could be complicated by the presence of nonlinear contributions to the anisotropies, arising from the late stages

[1]Also Department of Physics, University of Ljubljana, Jadranska 19, 61000 Ljubljana, Slovenia

of evolution. These are determined by different physical processes and are, because of the uncertainties in the nonlinear evolution, difficult to calculate even in well specified models. The most important contributions are the so-called Vishniac, Sunyaev-Zeldovich and Rees-Sciama effects. The first two effects are caused by Thomson scattering of photons off the free electrons moving in a bulk and random motion, respectively. They require an ionized medium and strongly depend on the ionization history of inter and intra-cluster medium, determined by the complicated physics of collisional gas (see e.g. Persi et al. 1995; Bond 1995 and references therein). The third effect, which is explored in this paper, is caused by a time dependent gravitational potential during the nonlinear stages of evolution. It does not depend on the ionization history of the universe, but only on the evolution of gravitational potential and is thus less model dependent.

The imprint of nonlinear clustering on the CMB was first pointed out by Rees & Sciama in 1968 and has subsequently been analyzed by several authors. Most of this previous work gave only partial answers, studying for example isolated structures, such as clusters, superclusters and voids (Rees & Sciama 1968; Kaiser 1982; Nottale 1984; Thompson & Vishniac 1987; Panek 1992; Martínez-González, Sanz & Silk 1990; Chodorowski 1992, 1994; Arnau, Fullana & Sáez 1994), quasi-linear (Martínez-González, Sanz & Silk 1992) or strongly nonlinear regimes (Martínez-González, Sanz & Silk 1994). Recently, Tuluie & Laguna (1995) presented a detailed N-body analysis of a standard CDM model using ray-tracing of photons. This approach has the advantage of producing real maps of $\Delta T/T$, thereby allowing one to identify the non-gaussian features that contribute to the Rees-Sciama effect. Unfortunately such approach is also computationally expensive and the results have a rather small dynamic range, in the case of Tuluie & Laguna (1995) being limited by the number of traced photons and by the resolution of their 64^3 PM simulation. For this reason these authors only present results on degree angular scales for one particular model.

The approach presented in this paper similarly uses output of N-body simulation to calculate the angular power spectrum of Rees-Sciama effect. The effect is calculated from the power spectrum using positions and velocities of particles in the simulation. This avoids the need to trace the photons through a dedicated N-body simulation and so it is not limited by the finite number of photons. Moreover, one can use already existing N-body simulations with large spatial resolution, allowing to calculate the effect with a much larger dynamic range. The range can be further extended to the scales larger than the size of simulation by matching the N-body results with the second order perturbation theory calculation, all of which allows one to calculate the effect with a high accuracy over most of the angular range of observational interest today. Another advantage of the approach used here is that several different CDM models can be analyzed with the same N-body simulation

by rescaling its time and length, which allows one to asses the sensitivity of the effect to the change in the shape and amplitude of the power spectrum. In section 2 I present all the necessary formalism to calculate the RS effect. In section 3 the formalism is applied to several CDM models, which is followed by discussion of the results and conclusion.

2. Power Spectrum of Potential Time Derivative

One can approximate the CMB temperature anisotropy $\Delta T/T(\vec{n}) \equiv \Delta(\vec{n})$ in the direction $\vec{n}$ as a contribution from the last scattering surface at recombination and a line-of-sight integral over the conformal time τ, (Sachs & Wolfe 1966; Martínez-González et al. 1990),

$$\Delta(\vec{n}) = \Delta(\vec{n})_{rec} + \int_{\tau_{rec}}^{\tau_0} 2\dot{\phi} d\tau, \tag{1}$$

where τ_{rec} is the recombination time, τ_0 the present time and first term $\Delta(\vec{n})_{rec}$ is the primary contribution to the CMB anisotropy created at the recombination. The second term on the right hand side is the integrated Sachs-Wolfe contribution and depends on the time derivative (with respect to the conformal time τ) of the gravitational potential ϕ along the line-of-sight. In the expression above the effect of Thomson scattering was neglected, which is valid if the dominant contributions to the integrated Sachs-Wolfe term come from low redshifts where the universe is optically thin independent of its ionization state. The integrated Sachs-Wolfe term and in particular its nonlinear contribution is usually associated with the RS effect. Note that the effect is frequency independent, because it is caused by the gravitational shifting of photons. This means that it cannot be separated from the primary contribution using a multi-frequency spectral information and the only way to identify it is to specify its spatial distribution.

The magnitude of the RS effect as a function of angle is studied in terms of the angular power spectrum C_l, which is defined as the l-th Legendre expansion coefficient of the correlation function,

$$C(\theta) = \langle \Delta(\vec{n}_1)\Delta(\vec{n}_2)\rangle_{\vec{n}_1\cdot\vec{n}_2=\cos\theta} = \sum_l (2l+1) P_l(\cos\theta) C_l, \tag{2}$$

where P_l is the l-th Legendre polynomial. Although for nonlinear processes studied here the power spectrum is not a sufficient statistic, it nevertheless provides a useful tool to compare contributions between various processes on the same angular scale, provided that they are statistically uncorrelated. Here I compare the anisotropies arising from the Rees-Sciama effect with the primary anisotropies arising at the recombination. The two

contributions are spatially well separated and can be treated as uncorrelated. In addition to this there might be other secondary contributions to CMB anisotropy Δ, such as the Sunyaev-Zeldovich or Vishniac effect mentioned above, both of which are also caused by the clustering of large-scale structure and are thus not necessary uncorrelated with RS effect. I will not discuss this general case here, since the main goal is to answer the question: can the RS effect dominate over the primary contribution on a given angular scale? If this indeed turns out to be the case, then a more detailed study of the RS effect would be needed, including the analysis of its higher order moments (e.g. Munshi, Souradeep & Starobinski 1994; Mollerach et al. 1995), producing real sky maps (e.g. Tuluie & Laguna 1995) and cross-correlating the RS effect with the other secondary sources that are important.

Expanding the potential time derivative $\dot{\phi}$ in the spherical basis and using orthonormality of spherical harmonics one obtains the following expression for the multipole moments of the RS effect in a flat universe (Seljak 1994),

$$C_l = (4\pi)^2 \int k^2 P_\phi(k) dk \left[\int_0^{\tau_0} 2\dot{F}(\tau) j_l(kr) \right]^2 d\tau. \tag{3}$$

$P_\phi(k)$ is the power spectrum of potential, $j_l(x)$ is the spherical Bessel function, $F(k,\tau)$ is the growth rate of potential and r is the comoving distance between the photon at a conformal time τ and the observer, $r = \tau_0 - \tau$. I assumed the distance to the last-scattering surface is given by $r \approx \tau_0$. Equation 3 is only valid in the linear regime, because of the assumption that a given mode is only changing in amplitude and not in phase, which allows a simple description of time dependence in terms of the growth factor $F(\tau)$, which is independent of the wavenumber. It also assumes that the relative separation between two photons is not affected by the gravitational lensing, a valid assumption on the scales of interest here (e.g. Seljak 1995).

The solution in equation 3 simplifies considerably if one is considering small angular scales and if the fluctuations at widely separated points can be considered statistically independent (a "fair sample" criterion). The latter condition is satisfied if the window function is broad compared to the largest correlation length, as it is the case in the late epoch of time dependent gravitational potential. Moreover, in this regime the correlations at a distance k^{-1} are slowly changing on a time scale $(ck)^{-1}$, because weak field gravity can only produce nonrelativistic motions. The radial integral in equation 3 is thus a product of a spherical Bessel function $j_l(kr)$ and a slowly changing function of time. This integral may be approximated by removing the slowly changing part and using the large l approximation,

$$\int_0^x j_l(x')dx' = \begin{cases} 0, & x < l \\ \sqrt{\frac{\pi}{2l}}, & x \geq l \end{cases} \tag{4}$$

Combining equations 3 and 4 one obtains

$$C_l^{(RS)} = 4(4\pi)^2 \int_0^\infty P_{\dot\phi}[k, \tau = \tau_0 - k/l)] \frac{\pi}{2l} S(k\tau_0 - l) dk = 32\pi^3 \int_0^{\tau_0} \frac{P_{\dot\phi}(l/r, \tau) d\tau}{r^2}, \quad (5)$$

where $S(x)$ is a step function being 0 below x and 1 above it. I introduced

$$P_{\dot\phi}(k, \tau) = \dot{F}^2(k, \tau) P_\phi(k), \quad (6)$$

the power spectrum of $\dot\phi$. Equation 5 is also valid in an open universe on small angular scales, provided that r is interpreted as the angular distance, $r = R \sinh[(\tau_0 - \tau)/R]$, where the curvature R can be expressed as $R = (1 - \Omega_0)^{-1/2} H_0^{-1}$, where H_0 is the Hubble constant today. The assumption that the power spectrum of $\dot\phi$ is not changing over a timescale $(ck)^{-1}$ guarantees the validity of equation 5 both in the linear and in the nonlinear regime (where both the amplitude and the phase of a mode are changing with time and the growth factor F depends on the wavenumber k). The slow time dependence in $P_{\dot\phi}$ may be restored when performing the radial integral in equation 5.

The power spectrum of $\dot\phi$ needs to be specified as a function of time and scale to compute the RS effect. The potential is related to the density through the Poisson equation, which in Fourier space is given by

$$-k^2 \phi = \frac{3}{2} \Omega_{m0} H_0^2 a^{-1} \delta. \quad (7)$$

Here Ω_{m0} is the matter density in units of critical density today, δ is the matter density perturbation and a is the expansion factor normalized to unity today. In the linear regime $\dot{F}$ is readily evaluated using the well known solution for the growing mode of density perturbations $D_+(\tau)$, $F(\tau) \propto D_+(\tau)/a(\tau)$ independent of k. For the zero curvature model with a cosmological constant ($\Omega_{m0} + \Omega_{v0} = 1$) the growth factor is given by (Heath 1977)

$$D_+(a) = \frac{\sqrt{\Omega_{m0} + \Omega_{v0} a^3}}{a^{3/2}} \frac{\int_0^a X^{3/2} da}{\int_0^1 X^{3/2} da}, \quad (8)$$

where $X = a/(\Omega_{m0} + \Omega_{v0} a^3)$ and $H_0 \tau = \int_0^a da/(\Omega_{m0} a + \Omega_{v0} a^4)^{1/2}$. In an open universe with no cosmological constant ($\Omega_{m0} < 1$, $\Omega_{v0} = 0$) the growth factor is (Heath 1977)

$$D_+(\tau) = -\frac{3 \sinh(\tau/R)[\sinh(\tau/R) - \tau/R]}{[\cosh(\tau/R) - 1]^2} - 2, \quad a = \frac{\Omega_{m0}}{1 - \Omega_{m0}} \frac{\cosh(\tau/R) - 1}{2}, \quad (9)$$

For closed universe ($\Omega_{m0} > 1$) the solution is obtained by analytic continuation and for flat case by Taylor expansion of equation 9 in the limit $R \to \infty$.

In a flat $\Omega_{m0} = 1$ universe $D_+(\tau) \propto a(\tau)$ and $P_{\dot{\phi}}(k)$ vanishes in the linear regime. In this case the lowest order contribution arises from the second order perturbation theory, where the density is expanded into $\delta = a\delta_1 + a^2\delta_2$, which gives

$$\dot{\phi} = -\frac{3}{2}\frac{H_0^2}{k^2}\dot{a}\delta_2. \tag{10}$$

The power spectrum of δ_2 is given by several authors (Peebles 1980; Martínez-González, Sanz & Silk 1992; notation of the paper by Jain & Bertschinger 1994 is used below),

$$P_{22}(k) = \int d^3q P_\delta(q) P_\delta(|\vec{k} - \vec{q}|) F_2^2(\vec{q}, \vec{k} - \vec{q}), \tag{11}$$

$$F_2(\vec{k_1}, \vec{k_2}) = \frac{5}{7} + \frac{2}{7}\left(\frac{\vec{k_1} \cdot \vec{k_2}}{k_1^2 k_2^2}\right) + \frac{\vec{k_1} \cdot \vec{k_2}}{2}\left(\frac{1}{k_1^2} + \frac{1}{k_2^2}\right), \tag{12}$$

where $P_\delta(k)$ is the linear density power spectrum. The power spectrum of the potential time derivative is then given by $P_{\dot{\phi}} = 9/4(H_0/k)^4 \dot{a}^2 P_{22}$.

In the fully nonlinear regime even the second-order perturbation theory breaks down and the behavior of the power spectrum $P_{\dot{\phi}}(k, \tau)$ as a function of time becomes more complicated. It can only be calculated using numerical N-body simulations. An output from an N-body simulation consists of the positions and velocities of the particles in the simulation box. From this one can calculate the (over)density field $\delta(\vec{r}) = \rho/\bar{\rho} - 1$ and momentum density field $\vec{p}(\vec{r}) = (1+\delta)\vec{v}$ on a fixed grid in the box by counting the number of particles and their velocities near each grid point. Fourier transformation of these quantities gives $\delta(\vec{k})$ and $\vec{p}(\vec{k})$; for simplicity I will drop their explicit k-dependence in the following. Taking the time derivative of the Poisson equation 7 and using the continuity equation

$$\dot{\delta} + i\vec{k} \cdot \vec{p} = 0, \tag{13}$$

one obtains the following expression,

$$\dot{\phi} = \frac{3}{2}\left(\frac{H_0}{k}\right)^2 \Omega_{m0} a^{-1}(\eta\delta + i\vec{k} \cdot \vec{p}), \tag{14}$$

where I introduced $\eta \equiv \dot{a}/a$. This relation connects the potential time derivative to the density and momentum density. By averaging over all different modes with the same amplitude k one obtains the power spectrum $P_{\dot{\phi}}$.

An example of various power spectra computed from a high-resolution simulation of a standard CDM (Gelb & Bertschinger 1994) is shown in figure 1. The spectra have been calculated at high enough redshift ($z = 4$) to be still in the linear regime for the long wavelengths and are multiplied by $4\pi k^3$ to obtain a dimensionless quantity. Dotted line

and dashed-dotted line show the power spectrum of δ and $i\eta^{-1}\vec{k}\cdot\vec{p}$, respectively. The two spectra agree on large scales, where the linear theory is a good approximation and gives $\delta \approx -i\eta^{-1}\vec{k}\cdot\vec{p}$. On smaller scales they start to deviate from one another with the divergence of momentum density having more power than the density on the same scale. The time derivative of potential $\dot{\phi}$ is proportional to the sum of the two quantities (equation 10) and is given by the solid line. It starts much lower than the density power spectrum, but eventually rises above it and becomes dominated by the divergence of momentum density. This shows that it is the motion of the matter that makes a dominant contribution to $\dot{\phi}$ in the nonlinear regime. The dashed line shows the corresponding spectrum from the second-order perturbation theory calculation. On large scales the two spectra agree well, except at the longest wavelength bin, where the disagreement is caused both by insuficient sampling of the largest mode and possibly by the absence of long-wavelength coupling in the N-body simulation. On smaller scales the N-body simulation power spectrum rises above the corresponding second-order perturbation case and leads to an increase in the RS effect compared to the second order calculation.

The agreement between the results of the N-body simulation and second-order perturbation theory as a function of expansion factor a is studied in figure 2. The second-order power spectrum grows as a^4 and at late times it eventually rises above the N-body spectrum on large scales. On smaller scales the N-body spectrum dominates over the second-order power spectrum. For $k < 1h$ Mpc^{-1} there is a qualitative agreement between the two predictions, which gives confidence that one may use the results from the second order perturbation calculation on scales larger than the size of simulation box. The discrepancy present at late times even at the longest wavelengths in the simulation could be caused either by the nonlinear effects beyond the second order or by the absence of long-wavelenth coupling in the simulation. It leads to some uncertainty in the final results, which are discussed in the following section.

Another approach used in the literature is to approximate the evolution of $\dot{\phi}$ using only the evolution of density (or potential) power spectrum (Martínez-González et al. 1994). For example, one could use semi-analytic approximations by Hamilton et al. (1991), which model the evolution of potential power spectrum and try to deduce the power spectrum of $\dot{\phi}$ using $P_{\dot{\phi}} = (d(P_\phi)^{1/2}/d\tau)^2$. This approximation assumes that for a given mode only its amplitude is changing with time, while its phase remains constant and is equivalent to the approximation used by Martínez-González et al. (1994). It gives valid results in the linear regime, but breaks down in the nonlinear regime. This is explicitly shown with the dashed-dotted curve denoted with MSS in figure 1, where one can see that it gives a poor agreement with the full treatment both in the perturbative and in the strongly nonlinear regime. In the second order perturbation theory the density power spectrum

receives contributions both from $\langle\delta_2\delta_2\rangle$ and from $\langle\delta_1\delta_3\rangle$. The two contributions are of the same magnitude and partially cancel each other (Jain & Bertschinger 1994), leading to a severe underestimation of $P_{\dot\phi}$. In the strongly nonlinear regime the power spectrum of $\dot\phi$ is dominated by the momentum density, which is determined by the momentum part of the single particle phase space. Its evolution is faster than the evolution of the density power spectrum, which is determined solely by the positions of particles, again leading to an underestimate of $P_{\dot\phi}$. Therefore, even with a correct time evolution of density power spectrum (which was not used by Martínez-González et al. 1994) one cannot obtain a reliable estimate of $P_{\dot\phi}$. For its proper description one needs to specify the full particle phase space information, given by both the density and the momentum density fields.

There is another Rees-Sciama contribution to the CMB anisotropies associated with the creation of vector metric perturbations. The effect on CMB is described by the vector component of the integrated Sachs-Wolfe term, $\Delta(\vec{n}) = \int_{\tau_{rec}}^{\tau_0} \vec{n}\cdot\dot{\vec{w}}d\tau$ (Sachs & Wolfe 1967), where $\vec{w}$ is the vector metric perturbation and is created by the transverse momentum density $\rho\vec{v}_\perp$ (e.g. Bertschinger 1995),

$$-k^2\vec{w} = 16\pi G a^2 \rho\vec{v}_\perp. \tag{15}$$

In the nonlinear regime vector perturbation is suppressed by v/c compared to the scalar perturbation, which has the density ρ as a source (equation 7). In the perturbative regime a more careful comparison is needed, because both contributions vanish in the lowest order. An estimate of the vector amplitude can be obtained by taking the time derivative of equation 15 and using the Euler's equation for $\rho\vec{v}$. This gives $\dot{w} \propto k\phi^2$, which has to be compared to $\dot\phi \propto k^2 H_0 \phi^2$ from equation 10 (with $\delta_2 \propto \delta_1^2$) for the scalar contribution. The vector contribution is thus suppressed by $(kH_0)^{-1} \ll 1$ relative to the scalar contribution and may safely be neglected as a source of CMB anisotropy both in the perturbative and in the strongly nonlinear regime.

3. Angular Power Spectrum of the Rees-Sciama Effect

The N-body results were obtained from a particle-particle/particle-mesh simulation of a standard CDM model with $\Omega_{m0} = 1$ and $H_0 = 50$ km/s/Mpc (Gelb & Bertschinger 1994). This is a $(50h^{-1}\mathrm{Mpc})^3$ simulation with 144^3 particles and a resolution of $32h^{-1}$kpc, normalized to linear $\sigma_8 = 1$ today (i.e. the linear mass overdensity averaged over spheres of radius $8h^{-1}$Mpc is unity today). The power spectrum of $\dot\phi$ was calculated on a 384^3 grid. No shot-noise subtraction was applied to the results and for this reason only the

lower half of k-modes were used in the actual analysis. The largest mode in the simulation was excluded because of insufficient sampling and/or large-scale cutoff problems. This resulted in the dynamic range of N-body simulation between 0.27 and $25h\mathrm{Mpc}^{-1}$ in k. For $k < 0.27h\mathrm{Mpc}^{-1}$ and $z > 9$ the second order perturbation theory calculation was used.

Although the N-body simulation was performed for the standard CDM model, one can change the parameters of the model without having to use a different simulation or even to recalculate the power spectrum of $\dot{\phi}$. For example, a change in the normalization amplitude σ_8 corresponds to a change in the expansion factor and N-body results at expansion factor a can be used as N-body results today for a different CDM model with $\sigma_8 = a$. Similarly we can also rescale the length, which corresponds to a change in the shape of the CDM power spectrum. To create a CDM model with $\Omega_{m0}h = 0.25$, which is the model that agrees best with recent large-scale structure surveys (e.g. Peacock & Dodds 1994; da Costa et al. 1994), one needs to rescale the distance by a factor of 2 and instead of $50h^{-1}$ Mpc box the size of simulation becomes $100h^{-1}$ Mpc. At the same time the normalization also changes, because $8h^{-1}$Mpc scale corresponds to a twice smaller scale in the box, which has more power than the original $8h^{-1}$Mpc scale. In such a model the output at $a = 0.61$ corresponds to today if $\sigma_8 = 1$. If one adopts $\sigma_8 = 0.6$ as suggested by cluster abundances (White, Efstathiou & Frenk 1993), then today corresponds to $a = 0.36$ in the original simulation.

Figure 3 shows the C_l's for various CDM models discussed above. In all cases the prediction for the temperature anisotropy Δ is between 10^{-7} and 10^{-6} over a large range of l, which is at least an order of magnitude below the predictions from the primary anisotropies in standard recombination CMB models. The RS anisotropies are sensitive to the normalization and shape of the power spectrum. To the extend that the second order theory is valid the amplitude scaling is given by σ_8^4 and so a change of σ_8 by a factor of 2 leads to more than an order of magnitude effect in C_l's [1]. For a given σ_8 a decrease in $\Omega_{m0}h$ gives more power to the large scales and the Rees-Sciama effect increases on large angular scales. This is particularly significant for low values of l where changing $\Omega_{m0}h$ by a factor of two leads to almost an order of magnitude effect in C_l, but is less important for $l \approx 1000$, which is dominated by the scales that contribute to the σ_8 normalization and so primarily depends on the amplitude of the power spectrum. For the model that best fits the present day clustering properties ($\Omega_{m0}h = 0.25$ and $\sigma_8 = 0.6$) the RS effect peaks at $l \approx 100$, where its power is three orders of magnitude below the primary signal. Even for the most extreme model studied here ($\sigma_8 = 1$ and $\Omega_{m0}h = 0.25$) the RS effect is two

[1]When comparing the RS effect to the primary anisotropies it is customary to normalize the primary contribution to COBE, which does not change with σ_8. Normalizing it to σ_8 the ratio between the two spectra scales as σ_8^2.

orders of magnitude weaker than the primary signal on degree scales and never exceeds $\Delta T/T \sim 10^{-6}$. Most models become significant in comparison with the primary anisotropies only around $l \approx 5000$ where $\Delta T/T \sim 10^{-7}$, well below the present observational sensitivity. For the standard CDM model the power spectrum obtained using only the second order calculation is also plotted on figure 3. It agrees with the full calculation on large scales, overestimates slightly the C_l's at intermediate scales ($300 < l < 3000$) and underestimates them at high l, where strongly nonlinear effects become dominant. In the regime where the primary anisotropies are important ($l < 1000$), second order calculation gives reliable results and may even overestimate the anisotropies, contrary to the expectation that it significantly underestimates them (Martínez-González et al. 1994).

Lack of N-body data on large and small scales leads to some uncertainty in the angular power spectrum. One can see from figure 2 that at late times there is some discrepancy between the second order calculation and N-body results even at long wavelengths and the extrapolation to the wavelengths larger than the box leads to some error in angular power spectrum. This is further investigated in figure 4, where the logarithmic contribution to C_l's as a function of wavenumber k (figure 4a) and redshift z (figure 4b) is shown for several values of l. For low l there is a discontinuity at $k = 0.27h\mathrm{Mpc}^{-1}$ caused by a poor matching of the two power spectra at late times. This discontinuity is the largest for values of l which receive the dominant contribution from the wavelengths around the box size at late epochs ($z < 1$). The uncertainty in C_l because of this is at most 20-30% for $l \approx 100$ and is significantly smaller at larger l. For large l the small scale cut-off limits the angular resolution of the RS effect. In principle the integral in equation 5 should be performed from the observer to the last-scattering surface, however due to the finite resolution in the N-body simulation one can only start to integrate from $r = l/k_{max}$, where in the present case $k_{max} = 25h\mathrm{Mpc}^{-1}$. For low l this results in a few Mpc cutoff in r, rising up to $400h^{-1}$ Mpc at $l = 10000$. At this value of l the dominant scale is $k \approx 5h\mathrm{Mpc}^{-1}$ (figure 4a) and the scales with $k > 25h\mathrm{Mpc}^{-1}$ still have a negligible contribution. Only for $l \gg 10000$ the scales smaller than $(25\mathrm{h})^{-1}$Mpc become significant and limit the dynamic range of angular power spectrum. The redshift distribution studied in figure 4b indicates that the typical contribution to the RS effect comes from z around 1 at $l > 1000$. At lower l the dominant contribution comes from redshifts below 1 (e.g. $z \approx 0.2$ at $l \approx 100$), but is never dominated by very nearby structures. This is comforting as it guarantees that the fair sampling criterion is satisfied. Moreover, the observational bias caused by observing areas of the sky which do not contain large nearby clusters should be small for all but the smallest values of l.

The conclusion derived from this paper is that in the models with no early reionization the Rees-Sciama effect is negligible compared to the primary anisotropies on

all observationally interesting scales ($\theta > 1'$) and is in any case below the present-day observational limits ($\sim 10^{-6}$ in $\Delta T/T$) on all angular scales. While the results presented here are specific to the flat CDM models, other models that reproduce the observed cluster abundance and large-scale correlations should give comparable results. The main additional effect present in the models with $\Omega_{m0} < 1$ is the decay of potential on linear scales (equations 5-9), which gives an important additional linear contribution to the CMB anisotropies on very large scales (Kofman & Starobinski 1985; Kamionkowski & Spergel 1994) and also on smaller scales in reionized models (Hu & Sugiyama 1994). The nonlinear RS effect itself actually decreases in low Ω_{m0} models because for a given density normalization both the linear potential and the linear velocity decrease with Ω_{m0} and lead to a smaller $\dot{\phi}$ (this will be partially offset by the longer comoving radial pathlength). The linear RS effect is also present in mixed or hot dark matter models, where massive neutrinos contribute to the dark matter and their free-streaming causes the potential to change in time at late epochs. This leads to a small, but potentially measurable effect on primary CMB anisotropies (e.g. Ma & Bertschinger 1995). If the universe was reionized early enough so that it became optically thick, then the primary anisotropies would have been erased and the RS effect would dominate over the primary contribution at a much lower l. However, in this case secondary anisotropies caused by the Vishniac effect would also be more important and would swamp the RS effect, as they give few times 10^{-6} contribution in the early reionized universe (e.g. Persi et al. 1995). Therefore, the Rees-Sciama effect is likely to be unimportant on arcminute scales and larger regardless of the particular model of structure formation or of its reionization history.

I would like to thank Ed Bertschinger for providing the N-body data and for many useful discussions, Bhuvnesh Jain for insights on the second order perturbation theory calculation and both for a careful reading of the manuscript. This work was supported by NSF grant AST-9318185 and NASA grant NAG5-2186. Supercomputing time was generously provided by the Cornell Theory Center and the National Center for Supercomputing Applications.

REFERENCES

Arnau, J. V., Fullana, M. J., & Sáez, D. 1994, MNRAS, 268, L17

Bertschinger, E. in "Cosmology and Large Scale Structure", Les Houches summer school, ed. R. Schaeffer, to be published (Elsevier Science Publishers, Netherlands)

Bode, P., & Bertschinger, E. 1995, preprint astro-ph 9504040

Bond, J. R. 1995, in "Cosmology and Large Scale Structure", Les Houches summer school, ed. R. Schaeffer, to be published (Elsevier Science Publishers, Netherlands)

Chodorowski, M. J. 1992, MNRAS, 259, 218

Chodorowski, M. J. 1994, MNRAS, 266, 897

da Costa, L. N., Vogeley, M. S., Geller, M. J., Huchra, J. P., & Park, C. 1994, ApJ437, L1

Gelb, J., & Bertschinger, E. 1994, ApJ, 436, 467

Hamilton, A. J. S., Kumar, P., Lu, E., & Matthews, A. 1991, ApJ, 374, L1

Heath, D. J., 1977, MNRAS, 179, 351

Hu, W., & Sugiyama, N. 1994, Phys. Rev. D, 50, 627

Hu, W., & Sugiyama, N. 1995, Phys. Rev. D, 51, 2599

Jain, B., & Bertschinger, E., 1994, ApJ, 431, 495

Kaiser, N. 1982, MNRAS, 198, 1033

Kamionkowski, M. & Spergel, D. N. 1994, ApJ, 432, 7

Kofman, L., & Starobinsky, A. 1985, Sov. Astron. Lett., 11, 271

Ma, C. P., & Bertschinger, E. 1995, ApJ, to be published

Martínez-González, E., Sanz, J. L., & Silk, J. 1990, ApJ, 355, L5

Martínez-González, E., Sanz, J. L., & Silk, J. 1992, Phys. Rev. D, 46, 4196

Martínez-González, E., Sanz, J. L., & Silk, J. 1994, ApJ, 436, 1

Mollerach, S., Gangui, A., Lucchin, F., & Matarrese, S. 1995, preprint

Munshi, D., Souradeep, T., & Starobinski, A. A. 1994, preprint IUCAA-38/94

Nottale, L. 1984, MNRAS, 206, 713

Panek, M. 1992, ApJ, 388, 225

Peacock, J. A., & Dodds, S. J. 1994, MNRAS, 267, 1020

Peebles, P. J. E., The Large Scale Structure of the Universe (Princeton University, Princeton, NJ, 1980)

Persi, F. M., Spergel, D. N., Cen, R., & Ostriker, J. P. 1995, ApJ, 442, 1

Rees, M. J., & Sciama, D. W. 1968, Nature, 517, 611

Sachs, R. K., & Wolfe, A. M. 1967, ApJ, 147, 73

Seljak, U. 1994, ApJ, 435, L87

Seljak, U. 1995, ApJ, submitted

Smoot, G. F. et al. 1993, ApJ, 396, L1

Thompson, K. L., Vishniac, E. T. 1987, ApJ, 313, 517

Tuluie, R., & Laguna, P. 1995, ApJ, 445, L73

White, S. D. M., Efstathiou, G., & Frenk C. S. 1993, MNRAS, 262, 1023

This preprint was prepared with the AAS LaTeX macros v3.0.

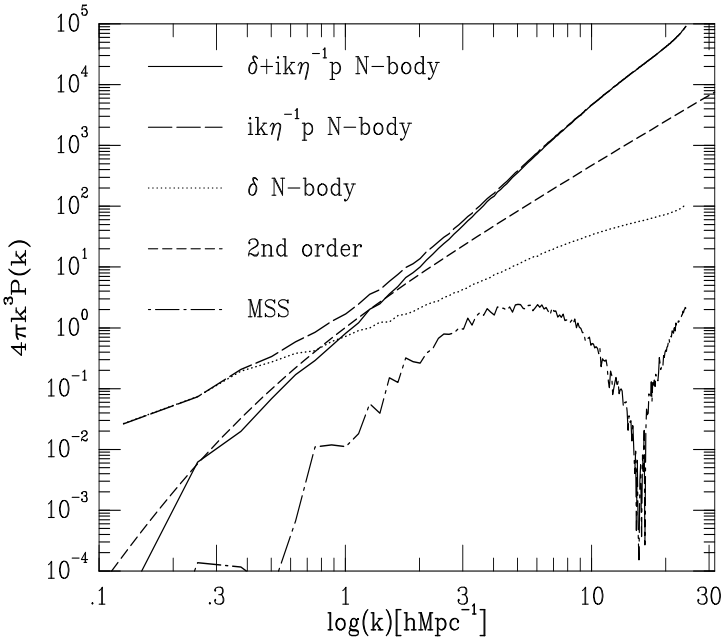

Fig. 1.— Comparison between various power spectra discussed in the text at $z = 4$. MSS denotes the Martínez-Gonzalez et al. (1994) approximation using the evolution of the density power spectrum alone. The curve was computed by finite differencing of two power spectra at different times and is noisier than other spectra, which are computed at the same time.

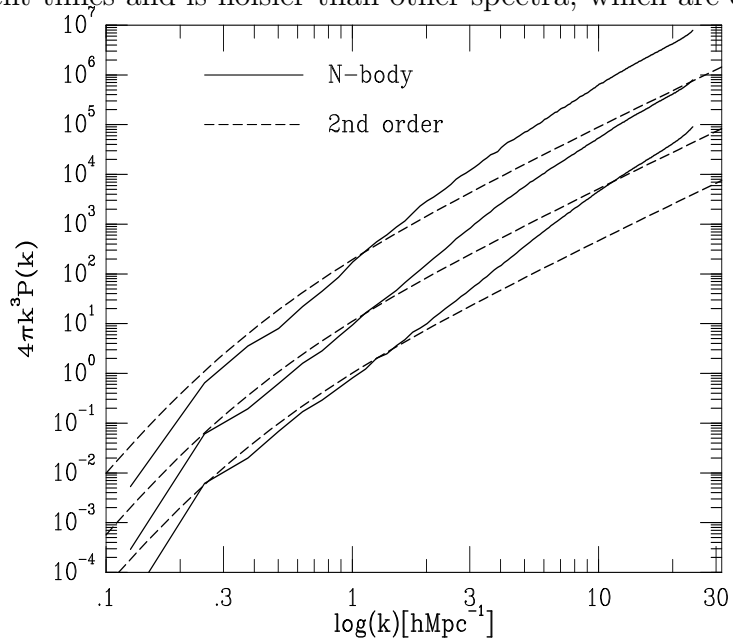

Fig. 2.— Comparison between N-body and second order calculation of $\delta + i\eta^{-1}\vec{k}\cdot\vec{p}$ as a function of expansion factor $a = (1+z)^{-1}$. From bottom to top the three spectra are for $a = 0.2$, $a = 0.4$ and $a = 0.8$, respectively.

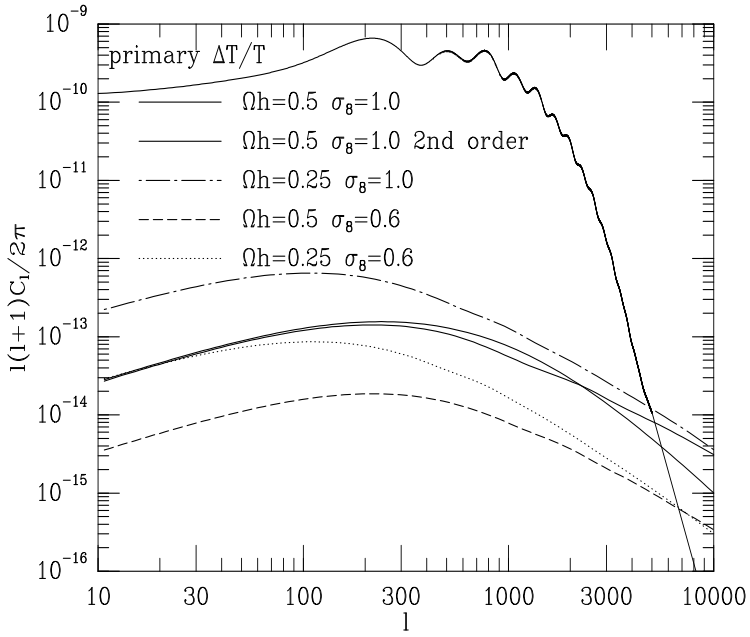

Fig. 3.— RS contribution to the angular power spectra $l(l+1)C_l/2\pi$ for various CDM models. Also plotted is the RS effect for the standard CDM case from the second order calculation and the primary contribution to the spectrum for a COBE normalized adiabatic CDM model ($h = 0.5$, $\Omega_{b0}h^2 = 0.05$), adopted from Bode & Bertschinger (1995).

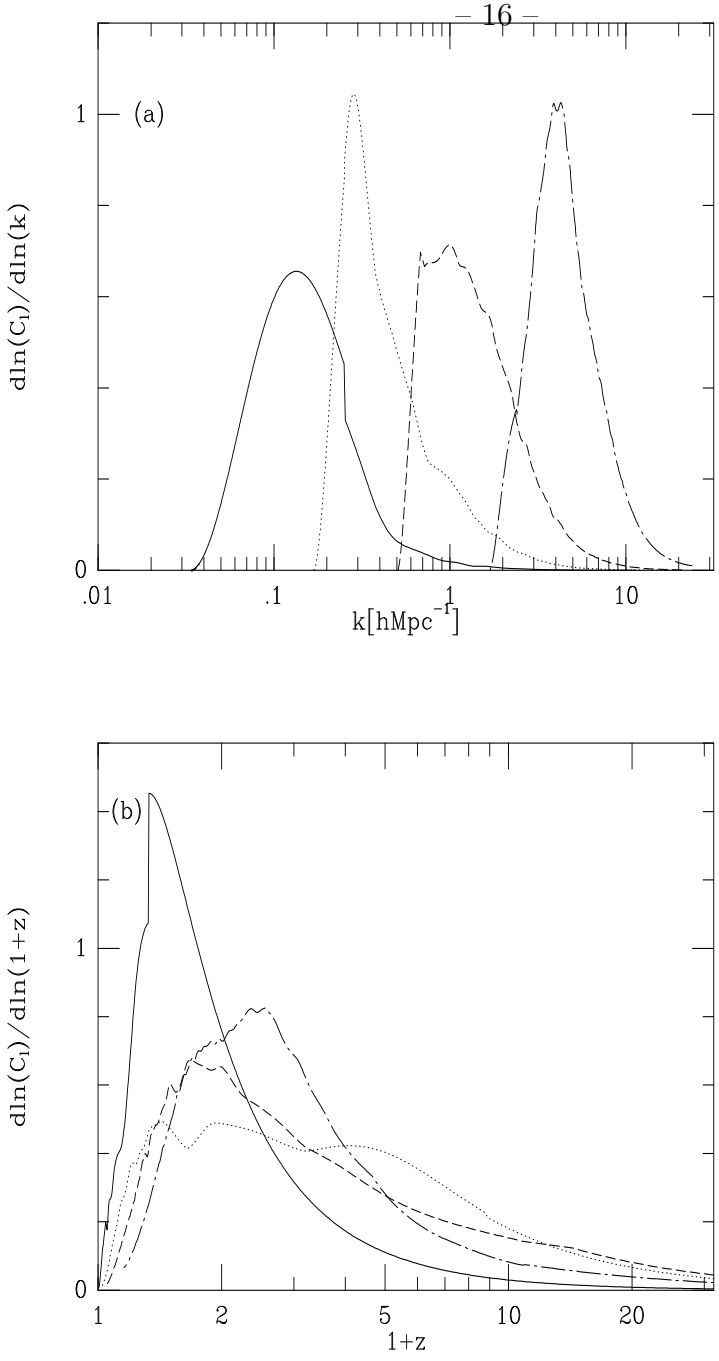

Fig. 4.— In (a), logarithmic contribution to C_l's is plotted as a function of wavenumber k for the standard CDM model. From left to right the l values are: 300, 1000, 3000 and 10000. In (b), logarithmic contribution to C_l's as a function of redshift z is plotted for the same values of l.